Feasibility Study of a 1000+ Electrode Array in Epiretinal Prosthesis

Diego Luján Villarreal, Dietmar Schroeder, and Wolfgang H. Krautschneider
Institute of Nano and Medical Electronics, Hamburg University of Technology, Hamburg, Germany
Email: {diego.lujan, d-schroeder, krautschneider}@tuhh.de

***Abstract*—To improve resolution and achieve functional vision, it is required 1000 electrodes with minimum feature size at epiretinal prosthetic devices. This challenging aim, however, has a limitation as to accommodate 1000+ electrode array and be within the limits of charge density and temperature increase at the device. In this work, we simulated a ganglion cell ON-model with PEDOT-NaPSS arranged electrode array in a three-dimensional retina model using COMSOL-Matlab interface. We varied electrode size, pulse width and inter electrode-ganglion cell distance to analyze charge density and temperature increase at the device. With our results, we investigated the feasibility of using 1024 electrode array attaching 16 scalable chips of 64 electrodes each with a daisy chain configuration. For I_{EGD} less than 10 µm, it is feasible to use 1024 array of electrodes with the following requirements: i) reduce electrode diameter to 2µm; ii) maximum output voltage of 1 V; iii) work with either 50 or 100µs low pulse duration; iv) 11.3mm^2 electrode carrier area; v) PEDOT-NaPSS electrode deposition and vi) circular electrodes.**

***Index Terms*—ganglion cell model, ionic current model, 1000 electrode array retinal prosthesis, electrode dimension limit**

I. Introduction

Epi- and sub retinal prosthetic devices strive to partially restore vision to those suffering retinal degenerative diseases such as age-related macular degeneration and retinitis pigmentosa. Though there have been notable progresses in this field, new devices may face further challenges for safely electrode implantation.

From theoretical modelling, it is estimated that a 1000+ electrode device could provide a decent functional vision, i.e. reading ability, object and face recognition [1].

It was demonstrated in [2] a novel scalable 64 channel stimulator to realize a fully implantable device of 1000+ electrodes for epi- or subretinal stimulation. Using that design, it is possible to attach 16 chips in daisy chain configuration with low area requirement, low power consumption and low residual charge using a 130 nm CMOS process and PEDOT-NaPSS electrode deposition.

Low power consumption can support large scale of Local Stimulation Units (LSUs) with less heat delivered by the device.

In this work, we simulated a single ganglion cell ON-model with PEDOT-NaPSS arranged electrode array using LivelinkTM for Matlab to integrate COMSOL Multiphysics®. Then, we investigated the feasibility of using 1024 electrodes by attaching 16 chips of 64 electrodes each in a daisy chain configuration as seen in [2].

Further, another enquiry investigated how the electrode size can be minimized and simultaneously be within the limits of charge density and temperature increase at the device. Our simulations have the following features:

i) 1024 electrode feasibility study.

ii) Low electrode diameter.

iii) Maximum output voltage study.

iv) Pulses shorter than 150 µs of duration which can replicate light-elicited spiking patterns; trigger solely a single spike with precise temporal pattern and send a more physiological signal to the brain [3].

v) PEDOT-NaPSS electrode array, where the active is surrounded by eight guards, to stress the isolation of the active electrode, to confine the stimulus current to a small volume around the ganglion cell and to minimize electrode cross-talk [4], [5].

vi) Safe charge density results taken from previously work [6] and temperature increase limitations.

vii) Epiretinal technique

viii) Circular electrodes that reduce elevated charge densities arising from irregular shapes [3]. Advanced electrode materials, e.g. conductive polymer like PEDOT-NaPSS [7] has the property to lower considerably the electrode impedance. While injecting similar amount of charge with low peak voltage, they reduce the power consumption required to activate neurons. For knowing the feasibility of this study, we varied electrode diameter, ED, pulse width, Δt, and inter electrode-ganglion cell distance, IEGD, in our simulations to analyze: i) charge density limitations [6], ii) high stimulus frequency limitations, iii) safely injecting current impulses without exceeding temperature increase limit at the device, iv) maximum output voltage of operation, v) lifting off of the array of electrodes from the retinal surface.

II. Methods

A. Assumptions

In our model, the assumptions are the following: i) our model consists of a single ON ganglion cell and its activation can be described by a single membrane potential (ON-model choice is clarified in Section II-B).

Manuscript received January 18, 2016; revised July 5, 2016.

doi: 10.18178/ijpmbs.5.3.163-170

ii) We excluded the retinal network model, i.e. bipolar, horizontal and amacrine cells, either ON- or OFF-network, because of severe rod and cone photoreceptor impairment that cannot drive synaptic connection started with a photocurrent input.

iii) Extracellular current density across the cell membrane at COMSOL simulations is equal as in the equivalent circuit of ganglion cell [8] which is modelled as voltage-gated channels. Hodgkin and Huxley-like equations can describe the eliciting of action potential at the cell membrane (section II-C).

iv) The sum of the power of the transistors that drive the electrodes and the power consumed per LSUs is sufficient to describe the total average power density of the device, P_{DEVAVE}, (section III-C).

B. Ganglion Cell Model Selection

Visual transmission beginning at the photoreceptors consists in the segregation of opposite light and dark signals into ON and OFF responses, depending on the bipolar cell types [9]. ON-pathway responds once a light image is pictured upon a darker background, e.g. night vision. OFF-pathway detects the opposite [10].

Retinitis Pigmentosa (RP), a leading cause of visual injury, affects primary the rod photoreceptors light sensitive cell [11] which are activated at low light levels. Rods selectively contact only with depolarizing ON bipolar cells and create ON visual pathways [12]. There may be some involvement on retinal cone cells, which detect bright light and provide color vision [11]. Recent findings support the evidence of preferential loss of ON-pathway during degenerative process of RP [13].

Age-related Macular Degeneration (AMD), a second cause of visual impairment, also experience poor night vision symptoms [14]. Further [15] suggest that assessing night vision symptoms may be useful to identify patients with early or intermediate AMD who are at relatively high risk of progression.

Since ON-pathway is preferentially impaired while being affected by RP or AMD, electrical stimulus via electrode array is required for restoring light sensitive cells performance and for improving visual transmission. Therefore, ON-ganglion cell model is selected because ON-pathway is more affected by the diseases previously mentioned.

C. Ganglion Cell Model in Matlab

Ganglion cell model has a basic mathematical structure for voltage-gating based on Hodgkin and Huxley like equations [16] and is modelled with an equivalent circuit taken from previously published model of repetitive firing of retinal ganglion cells [8].

The parameters and equations that describe the dynamics of the ionic channels were kept as in the original model.

Four conductances associated to voltage-gated channels were considered: calcium gCa channel; sodium gNa channel; non-activating K+ (delayed rectifier) gK; inactivating K+ (A type) gaK; calcium-activated K+ gkCa channel was gated by calcium Ca2+ and modelled on that basis. OFF- and ON-ganglion cells receive the signal separately, satisfying parallel pathways of OFF- and ON-bipolar cells and amacrine cells [12]. For our circumstance, we used ON-ganglion cell model.

D. Retinal 3D Model in COMSOL

The 3-dimensional model of the retina is shown in Fig. 1 as a 2-dimensional cross section.

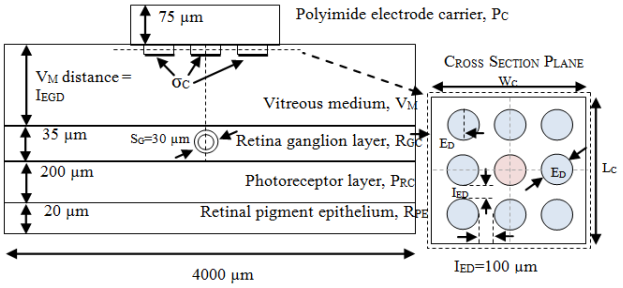

Figure 1. Retina model at COMSOL simulations. Layer thickness not drawn to scale.

Our model consists of seven domains: polyimide carrier of electrodes P_C; vitreous medium V_M; retina ganglion cell layer R_{GC}; photoreceptor layer P_{RC}; retinal pigment epithelium R_{PE}; ganglion cell soma S_G and the electrode array. The ganglion cell soma was placed inside the retina ganglion cell layer exactly below the center of active electrode and was enclosed with the cell membrane.

The extracellular and intracellular compartments of the membrane were modelled with their respectively electrical properties. In order to reduce the impedance of electrodes and to emphasis biocompatibility, the materials selected were PEDOT-NaPSS electrodeposited in gold electrodes with a charge density of 40mC/cm^2 [7]. Gold and PEDOT polymer are good conductors with 41e6 and 40e3 S/m of conductivity, respectively.

From [7], we used the Bode diagram of a set of 24 electrodes which were divided in three groups of eight fabricated with diameters of 0.5, 1 and 2mm^2.

Then, we used the double-layer equivalent circuit model to characterize the contact interfaces of both materials, see Fig. 2, and to perform precise numerical fitting using ZView software.

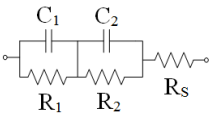

Figure 2. Double-Layer model for gold-PEDOT electrode configuration.

C_1 is related to the accumulation of charge between metal and polymer and R_1 is considered a contact resistance. R_S is the bulk resistance of the solution.

C_2 is the double-layer capacitance defining the accumulation of charge between the polymer and the solution and R_2 is the reaction resistance describing the charge transfer to the solution.

Numerical fitting results showed that the average contact resistance between PEDOT-NaPSS and the solution, R_2, is 8.6kΩ and 30 times greater than R_1.

Therefore, to reduce computational effort and time consumed, we omit the electrode domain of gold at

COMSOL simulations and we assumed solely to include the PEDOT-NaPSS deposition at the polyimide carrier. This assumption reduced the time consumed to 2.5 minutes.

The dimensions of the model were similar to previously published models [17]-[19]. The model geometry consisted of 4000 x 4000 μm at its bottom area. PEDOT-NaPSS electrode array as seen in [20] was fabricated with charge density of 40mC/cm^2 electrodeposition.

PEDOT-NaPSS deposition and cell membrane were constructed in COMSOL using the boundary layer feature where it was needed only the thickness of 200nm and 5nm, respectively, and electrical properties of 40e3 S/m, ε = 1 and 1e-8 S/m, ε = 8.8e-11, all respectively. The intracellular of soma properties are 0.09 S/m and ε = 3.98e-11.

The length and width of the polyimide carrier was dependent of the electrode diameter, E_D, and the edge of inter electrode distance, I_{ED}, of 100 μm as $W_C = L_C = 2(I_{ED}+2E_D)$.

The experimental data of [17]-[22] were utilized to obtain the proper conductivity and permittivity, all respectively, of the domains previously mentioned: 1.5 S/m and 98 for vitreous medium; 1e-17 S/m and 1 for polyimide carrier of electrodes; 40e3 S/m and 1 for PEDOT-NaPSS electrode array; 0.1 S/m and 80 and for retinal ganglion cell layer; 2e-3 S/m and 1 for retinal pigment epithelium and 28.5e-3 S/m and 1 for photoreceptor layer.

The contact conductivity, σ_C, between PEDOT-NaPSS and tissue was calculated as $1/(R_2*A_C)$, where A_C is the cross section area of the electrode and R_2 is the reaction resistance where the slope of R_2 versus A_C in log-log scale resembles a $1/A_C$ shape. Hence, σ_C is 321S/m^2.

The electrode array configuration is shown at the cross section plane in Fig. 1.

This arrangement is analogous to [4], [5], however it consists of an active electrode (in red) surrounded by eight guards (in blue) in order to stress the isolation of the active electrode, to confine the stimulus current to a small volume around the ganglion cell and to minimize electrode cross-talk during stimulation. We used the electric current study at COMSOL simulations.

E. Simulation Procedure: Ganglion Cell in Matlab

Ganglion cell model comprises the calculation of extracellular threshold current density of the ganglion cell using its model explained at Section II-C. The extracellular threshold current density of ganglion cell was found by injecting current density to the ganglion cell with pulse duration of 50, 100 μs and applied at 500 pps, taking into account absolute and refractory period of an action potential. We used monophasic rectangular pulse waveform. The peak current amplitude was swept with a resolution of 1 μA/cm^2 until it was found the threshold current density that fires a train of action potential. The results of strength duration curve at extracellular peak current amplitude are 330 and 120 μA/cm^2 for 50 and 100 μs, respectively.

F. Simulation Procedure: Retina Model in COMSOL

The retinal model was built in COMSOL and is shown in Fig. 1. After obtaining the extracellular peak current amplitude that fires a train of action potential at the ganglion cell, those results were used to match the average boundary current density of the cell membrane in the ganglion cell soma at COMSOL simulations.

In our simulations, we varied the Δt, E_D and I_{EGD} to analyse: i) charge density limitations [6]; ii) high stimulus frequency limitations; iii) safely injecting current impulses without exceeding temperature increase limit of 1 ℃ and iv) maximum output voltage of operation. The pulse widths tested are identical as Section II-E, i.e. 50, 100 μs, and it was used monophasic rectangular pulse for electrical stimulation.

Pulse durations lower than 150 μs are analogous in [3] to directly stimulate the ganglion cell and to elicit solely a single spike with precise temporal pattern. The inter electrode-ganglion cell distance, i.e. the variation of V_M, is 2, 10 and 100 μm. This variation is in order to simulate the changeability of threshold current and charge density due to the lifting off of the electrode array from the retinal ganglion cell layer surface. The values simulated are analogous to the experimental findings in [19]. The electrode diameter tested are 2, 10, 50 and 100 μm and are analogous to [3], [17], [23], [24].

G. Flowchart of Simulation

Fig. 3 shows the flowchart of our simulation procedure.

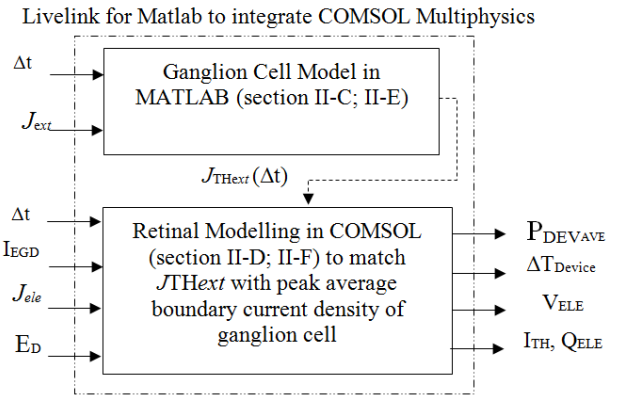

Figure 3. Flowchart of simulation.

The variables listed are the following: Δt is the pulse duration mentioned in Sections II-E and II-F.

J_{ext} is the extracellular current density injected to the ganglion cell mentioned in Section II-E; J_{THext} is the extracellular threshold current density which needs to match with the peak average boundary current density of ganglion cell at COMSOL simulations. I_{EGD} is the inter electrode ganglion distance mentioned in Section II-F; J_{ele} is the current density applied at the electrodes in COMSOL simulations; E_D is the electrode diameter stated in Section II-F; P_{DEVAVE} is the average power density at the device mentioned in the Section III-C; ΔT_{Device} is the change of temperature; V_{ELE} is the electrode voltage; I_{TH} and Q_{ELE} are the threshold current and the charge density from the electrodes.

III. Results

Out of COMSOL simulations we obtained the current density and voltage across the electrodes over time.

A. Threshold Charge Density

In Table I we list the summary of threshold charge density results from [6]. The threshold current is shown in Fig. 4 for a specific inter electrode-ganglion cell distance and pulse duration.

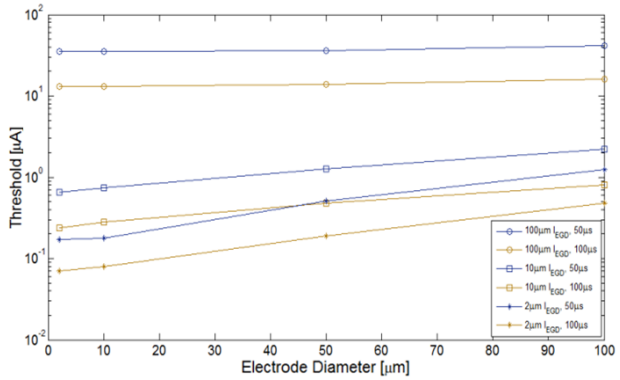

Figure 4. Threshold current for 2, 10, 100 μm of I_{EGD} at 50, 100 μs.

The charge density was obtained by integrating the current delivered by the center electrode over time and dividing it by the electrode area. It is worth to mention that all eight surrounding electrodes including the active changed their dimensions accordingly.

The limits of safe charge density are 0.35mC/cm^2 [25] and 1mC/cm^2 [26].

B. ASIC Attachment

As seen in Fig. 5, the proposed ASIC attachment is shown.

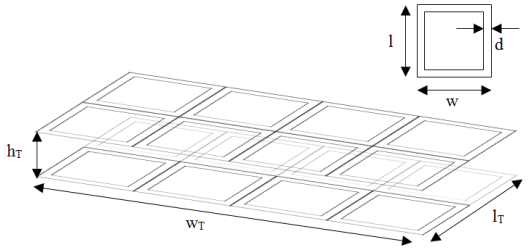

Figure 5. Two-Layer arragment of 16 chips attached in daisy configuration.

The area of one ASIC consists of the dimensions seen in [2] of 1.92mm x 2.2mm for a single chip and the distance, 'd', on each edge of 1 mm for wire bonding. The total width, 'w', and the length, 'l', of a single ASIC is 3.94 and 4.2mm, all respectively.

We selected a two layer arrangement of 2x4 each to minimize the total area of their attachment. In total we have 16 chips of 64 electrodes each. The total width, 'w_T', the length, 'l_T' and of one layer arrangement is 15.7 and 8.4mm, respectively. The total area of a single layer is 1.32cm^2. The height, h_T, between the layers is 1mm.

C. Power Consumption Analysis

The main objective of retinal stimulation, using either epi- or subretinal technique, is to provide functional vision that comes from 1024 image pixels with at least 20 images per second. To achieve this request, we studied the feasibility of using 1024 electrode array attaching 16 scalable chips of 64 electrodes each with a daisy chain configuration as seen in [2] with low power consumption of 54 μW per Local Stimulation Unit (LSU).

The stimulation waveform has a monophasic rectangular shape with a total image frequency, f, of 20 Hz. The main target is, within a time duration of 1/f, to individually trigger 1024 pixels with pulse duration Δt and have a full image. As seen in [2], each electrode can have a different timeslot. To achieve the main target, however, we could have a limitation to complete a full image of 1024 pixels within 1/f and with a known Δt, assuming that each electrode triggers one pixel.

We can calculate the minimum number of electrodes activated per Δt as $e_{ON} = 2(e_T*f*\Delta t)$. e_T is the total number of pixels considered, i.e. 1024 for our specific case. Δt is the pulse width. The total number of active electrodes, e_{AN}, can be computed as $e_{ON}/2$ and are activated per Δt.

The device activation is shown in Fig. 6 as 'a', and corresponds to the triggering of active electrodes.

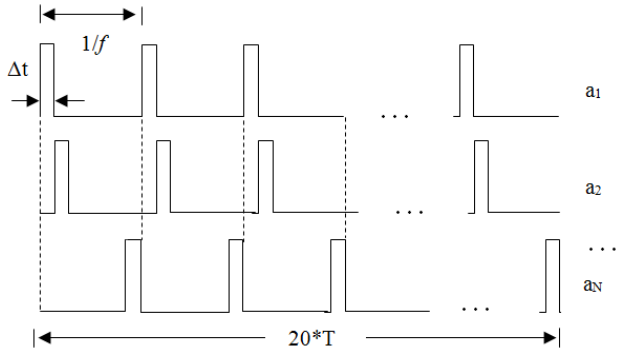

Figure 6. Waveforms for e_T/e_{AN} number of activations.

The total number of device activations, a_N, is equal to e_T/e_{AN}.

The average power density of the device, P_{DEVAVE}, is calculated considering the power of the transistors that drive one of the electrodes, P_T, during the pulse of stimulation and the power per Local Stimulation Unit (LSU), P_{LSU}.

P_T is calculated using a simplified electrical circuit of a retinal implantable device powered by a voltage source V_{DD}, see Fig. 7.

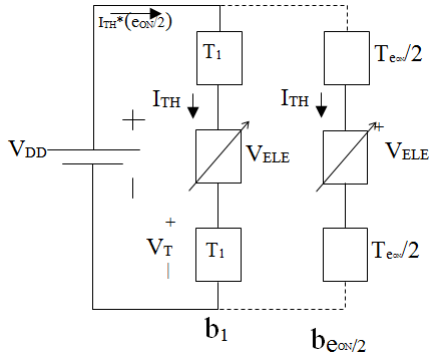

Figure 7. Simplification of implantable device circuitry.

Each branch, 'b', has two transistors which drives the active and ground electrodes and the load which is associated to the tissue.

For sake of simplicity, we assumed that the voltage drop in the tissues is equal to the voltage drop across the electrodes, V_{ELE}. Since each active or ground electrode is equivalent to one transistor as seen in [2], the total number of transistors is equal to e_{ON}. Since each branch contains two such transistors, the total number of branches is $e_{ON}/2$. The branches are activated per Δt.

V_T is the voltage drop in the transistors that drive the electrodes. I_{TH} is the threshold current. P_T is given by:

$$P_T = I_{TH}(V_{DD} - V_{ELE}) \quad (1)$$

We assume that the voltage drop in the branches is approximately the same and there is an equal distribution of current across the branches. The average power density at the device with units of [mW/cm^2] then is computed as follows:

$$P_{DEVave} = \frac{e_T \Delta t}{A_D T}(P_T + 2P_{LSU}) \quad (2)$$

Δt/T defines the duty cycle of stimulation. Δt is the pulse duration and T is the inverse of the total image frequency of 20Hz. A_D is the total chip surface area of 0.68cm^2 and P_{LSU} is the power consumption per electrode or LSU of 54 µW as seen in [2].

The neural tissue heating from the retina implant is calculated using the average power density at the device, P_{DEVAVE}, in the linear approach of ΔT = 1°C per 12.2mW/cm^2 [27] assuming only heat conduction. The initial temperature was body temperature of 37 °degrees.

Fig. 8 to Fig. 10 show the change of temperature increase at the device, left y-axis, and the electrode potential, right y-axis, for each case.

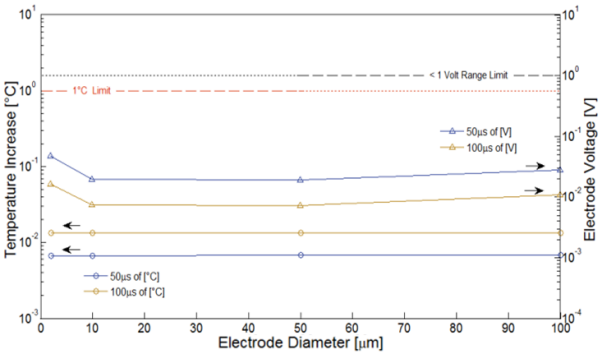

Figure 8. Temperature increase and electrode voltage for 2 µm I_{EGD}.

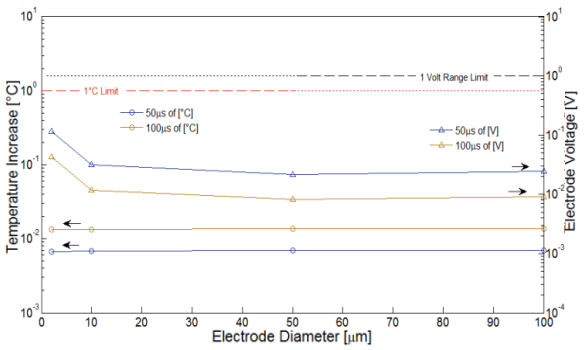

Figure 9. Temperature increase and electrode voltage for 10 µm I_{EGD}.

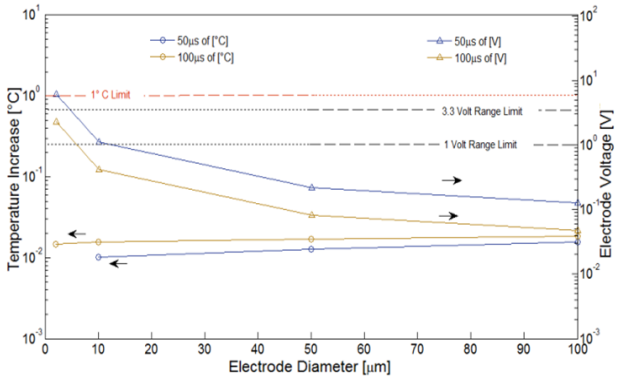

Figure 10. Temperature increase and electrode voltage for 100 µm I_{EGD}.

We used the voltage across the electrodes shown in Fig. 8 to Fig. 10, right y-axis, as the maximum output voltage of operation while stimulating the retina. Then, we compared it with the voltage supply of 3.3 V_{DD}, and 1 V_{DD} as a condition boundary of the voltage of operation.

D. 1024 Electrode Array

A 1024 electrode array can be assembled with an area computed as $A_{EC} = (33*I_{ED}+32*E_D)^2$, with each electrode homogeneously distributed in the carrier, see Fig. 11.

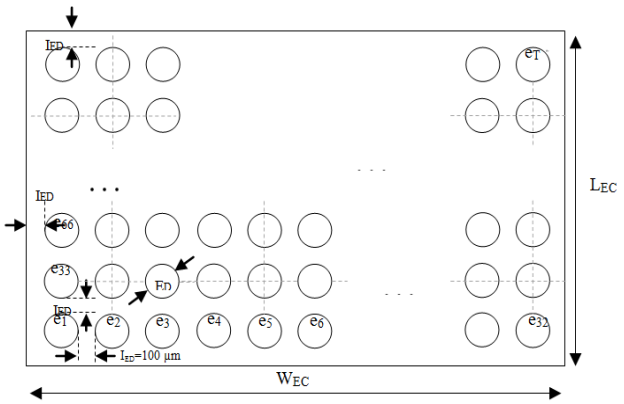

Figure 11. e_{32} x e_{32} electrode array. e_T = 1024 electrodes.

Assembling the electrodes evenly gives the advantage to program each to function as an active or ground electrode and to determine the optimal configuration of ganglion cell stimulation per each case. When an edge electrode is selected as active, its surrounding can be used as ground. Nevertheless, an unwanted effect of stimulating more ganglion cells may occur because of an uneven current density distribution.

The width, W_{EC}, and the length, L_{EC}, of the carrier can be computed as $A_{EC}^{0.5}$. For E_D from 2 to 100 µm and knowing I_{ED} of 100 µm to be constant, the electrode carrier area of 1024 evenly distributed electrodes is in the range from 11.3 to 42.2mm^2. Using the total area of the attachment seen in Section III-B of 1.32cm^2, the electrode carrier area would occupy from 8 to 31% of the total area of the chip arrangement.

A large electrode carrier area, however, has its own advantages. The visual field is directly related to the size of stimulated area of the retina and hence the diameter of the electrode array. The projected visual field for every 1mm of the retina is about 3.35 °[28]. For our case, it will

provide a central vision with a field of view of about 11 °×11 ° for 11.3mm^2 to 21 °×21 ° for 42.2mm^2.

Currently, electrode arrays implanted in animals or humans range from 9mm^2 to 33mm^2 in area [29]-[31]

IV. Discussion

A. Charge Density Limitations

Table I lists the summary of threshold charge density results taken from earlier work [6], and shows the minimum electrode diameter [μm] that can be used with their corresponding limit.

TABLE I. Summary of Charge Density Limit Results

	0.35mC/cm^2 limit		1mC/cm^2 limit	
	50 μs	100 μs	50 μs	100 μs
2 μm	Yes	Yes	Yes	Yes
10 μm	Yes	Yes	Yes	Yes
100 μm	18	14	9.7	9.6

The green boxes indicate the suitability to use the minimum electrode diameter tested of 2 μm. For a successful implant of retinal device, only the lower safe charge density of 0.35mC/cm^2 should be employed.

Assuming a PEDOT voltage window limit of 1.7V [32], a theoretical safe charge density of 0.35mC/cm^2 for gas-free and erosion-free operation and 1mC/cm^2 for neural damage, our simulations suggest that it is safe to inject current density for all electrode sizes and pulse widths tested within 10 μm I_{EGD}. Doing so, it provides a method to send a more natural signal to the brain and to generate meaningful percepts [3].

From [6], the simulations also suggest that decrease E_D to 14 μm using pulses of 100 μs at 100 μm I_{EGD} is safe within the limits. Reducing electrode size can be advantageous for stimulating the retina because they produce more focal stimulation. The main limitation, however, is high charge densities that can cause adverse tissue reactions.

Additional experimental testing of small electrodes is still required to verify our results.

Decreasing electrode dimension will generate, however, higher resolution patterns of prosthetic-elicited activity that are closer to light-elicited patterns and improve visual reception [23].

B. Threshold Current

Threshold currents were found to increase with time after surgery, most likely due to the lifting off of the electrode array from the retinal surface [1], see Fig. 4.

Experimental findings [33] confirm that this anomaly was particularly noticeable in the first postoperative weeks. As seen in Fig. 4, our results confirm higher threshold current at greater distances and are consistent with previous experimental work of epiretinal device implanted in rabbits [34].

C. Temperature Increase

Power consumption in retinal stimulator devices is restricted firstly because it is powered by an inductive coupling and secondly because it is associated with temperature increase at the device.

Fig. 8 to Fig. 10, left y-axis, show the change of temperature at the device.

For each case, the change of temperature slightly rises as the electrode diameter increases. This tendency can be attributed to the influence of electrode impedance and therefore the rise of its voltage which sequentially decreases the voltage at the device and its power consumption (see Fig. 7).

As aforementioned, that influence states an advantage to work with short pulse durations unless the electrode voltage does not exceed V_{DD}.

As seen in Fig. 8 to Fig. 10, all temperature results are below the range of 1 ℃ and they do not exceed the temperature limit. This behavior can be attributed to the use of the duty cycle and few LSU per Δt.

Assuming a linear approach of heat increase of 1 ℃ per 12.2 mW/cm^2, our simulations suggest that it is within the safe limits to deliver stimulus using 2 μm electrode diameter and to work with 50 and 100 μs pulse duration

D. Maximum Output Voltage of Operation

Seeing Fig. 7, we used the voltage across the electrodes as the maximum output voltage of operation while stimulating the retina. Then, we compared it with the voltage supply of 3.3 V_{DD}, and 1 V_{DD} as a condition boundary of the voltage of operation. As seen in Fig. 8 to Fig. 10 at right y-axis, it is shown the electrode voltage as the maximum output voltage of operation.

Table II lists the results for both limits, and indicates the minimum electrode diameter [μm] for the corresponding condition boundary. The green boxes indicate the suitability to use 2 μm electrode diameter.

TABLE II. Condition Boundary of Voltage of Operation

	1 V_{DD}		3.3 V_{DD}	
	50 μs	100 μs	50 μs	100 μs
2 μm	Yes	Yes	Yes	Yes
10 μm	Yes	Yes	Yes	Yes
100 μm	15.5	7.5	6.5	Yes

V. Conclusion

In this work, we investigated the feasibility of using a novel scalable 64 channel stimulator [2] to realize a fully implantable device of 1024 electrodes for epi- or subretinal stimulation.

For a given I_{EGD} and assuming safe temperature increase of 1 ℃ and charge density of 0.35mC/cm^2, our model suggests that is feasible to use 1024 array of electrodes with the following requirements:

i) $0<I_{EGD}<10$ μm: a) reduce electrode diameter to 2 μm; b) maximum output voltage of operation of 1V; c) work with either 50 or 100 μs low pulse duration; d) 11.3mm^2 electrode carrier area.

ii) $10<I_{EGD}<100$ μm: a) reduce electrode diameter to 14 μm only with 100 μs pulse duration. For 50 μs, electrode diameter should be 18 μm; b) maximum output voltage of operation of 1V for both cases; c) 14mm^2 for 14 μm and 15mm^2 for 18 μm electrode carrier area.

Each configuration works with PEDOT-NaPSS electrode deposition and circular electrodes.

To avoid further issues caused by implantation of an epi-, sub-retinal or suprachoroidal implant, the inter electrode-ganglion cell distance plays a major role for a successful retina implant. The major limitation, however, is attributed to the charge density required to elicit activity in neurons

REFERENCES

[1] G. Chader, J. Weiland, and M. S. Humayun, "Artificial vision: Needs, functioning, and testing of retinal electronic prosthesis," *Progress Brain Research*, vol. 175, pp. 317-332, 2009.

[2] M. Meza-Cuevas, D. Schroeder, and W. H. Krautschneider, "A scalable 64 channel neurostimulator based on a hybrid architecture of current steering DAC," in *Proc. Middle East Conference on Biomedical Engineering*, 2014.

[3] S. Fried, H. A. Hsueh, and F. S. Werblin, "A method for generating precise temporal patterns of retinal spiking using prosthetic stimulation," *J. Neurophysiol.*, vol. 95, pp. 970-978, 2006.

[4] N. Lovell, S. Dokos, S. L. Cloherty, and P. J. Preston, "Current distribution during parallel stimulation: Implications for an epiretinal neuroprosthesis," *IEEE Eng. Med. Biol. Soc.*, 2005.

[5] N. Dommel, *et al.*, "A CMOS retinal neurostimulator capable of focussed, simultaneous stimulation," *J. Neural Eng.*, vol. 6, p. 035006, 2009.

[6] D. L. Villarreal, D. Schroeder, and W. H. Krautschneider, "Charge density study using low electrode diameter in epiretinal prosthesis," in *Proc. ICTOpen2016 Conference*, Amersfoort, The Netherlands, March 22-23, 2016.

[7] R. Starbird, *et al.*, "Electrochemical properties of PEDOT-NaPSS galvanostatically deposited from an aqueous micellar media for invasive electrodes," in *Proc. IEEE BMEICON*, 2012.

[8] J. Fohlmeister, P. A. Coleman, and R. F. Miller, "Modeling the repetitive firing of retinal ganglion cells," *Brain Research*, vol. 510, pp. 343-345, 1989.

[9] S. Nakanishi, "Processing and integration mechanisms of visual transmission in the retinal network," in *The Neural Basis of Early Vision*, Springer Science & Business Media, 2013.

[10] C. Kristensson, "Evaluation of the retinal ON and OFF responses in the dog ERG," Faculty of Veterinary Medicine and Animal Science Department of Clinical Sciences, 2014.

[11] D. Maureen, "Optogenetics: Can this innovative gene therapy treat degenerative retinal disease and possibly restore sight?" 2015.

[12] J. R. Stephen, *et al*., *Retina*, Elsevier Health Sciences, 2012.

[13] J. Fransen, "The retina-prosthesis interface in two rat models of retinitis pigmentosa and functional changes associated with photoreceptor loss," Dissertation, 2013.

[14] L. Kathryn, *et al.*, *Pathophysiology: The Biologic Basis for Disease in Adults and Children*, Elsevier Health Sciences, 2015.

[15] G. Ying, M. G. Maguire, C. Liu, and A. N. Antoszyk, "Night vision symptoms and progression of age-related macular degeneration in the complications of AMD prevention trial," *Ophthalmology*, vol. 115, no. 11, 2008.

[16] A. Hodgkin and A. F. Huxley, "A quantitative description of membrane current and its application to conduction and excitation in nerve," *J. Physiol.*, vol. 117, pp. 500-544, 1952.

[17] P. Werginz, H. Benav, E. Zrenner, and F. Rattay, "Modeling the response of ON and OFF retinal bipolar cells during electric stimulation," *Vision Research*, vol. 111, pp. 170-181, 2004.

[18] M. Abramian, N. H Lovell, J. W. Morley, G. J. Suaning, and S. Dokos, "Computational model of electrical stimulation of a retinal ganglion cell with hexagonally arranged electrodes," in *Proc. 34th Annual International Conference of the IEEE EMBS*, 2012.

[19] H. Kasil, W. Hasenkamp, G. Cosendai, A Bertsch, and P. Renaud, "Simulation of epiretinal prostheses - Evaluation of geometrical factors affecting stimulation thresholds," *Journal of Neuroengineering and Rehabilitation*, vol. 8, no. 1, 2011.

[20] R. Starbird, "Study of organic materials to improve electrical properties of neural stimulation electrodes," Dissertation, 2013.

[21] S. Yin, N. H. Lovell, G. J. Suaning, and S. Dokos, "A continuum model of the retinal network and its response to electrical stimulation," in *Proc. IEEE EMBS*, 2010.

[22] T. Kameneva, H. Meffin, and A. N. Burkitt, "Modelling intrinsic electro physiological properties of ON and OFF retinal ganglion cells," *J. Comput. Neuroscience*, vol. 31, no. 3, 2011.

[23] C. Cai, Q. Ren, N. J. Desai, and S. I. Fried, "Response variability to high rates of electric stimulation in retinal ganglion cells," *J. Neurophysiology*, vol. 106, pp. 153-162, 2011.

[24] J. Rizzo III, J. J. Wyatt, S. Kelly, and D. Shire, "Methods and perceptual thresholds for short-term electrical stimulation of human retina with microelectrode arrays," *IOVS*, vol. 44, no. 12, 2003.

[25] S. B. Brummer and M. J. Turner, "Electrical stimulation with Pt electrodes. II. Estimation of maximum surface redox (theoretical non-gassing) limits," *IEEE Trans. Biomed. Eng.*, 1977.

[26] E. W. Finn and P. Lopresti, *Handbook of Neuroprosthetic Methods*, CRC Press, Dec. 16, 2002.

[27] S. Kim, R. A. Normann, R. Harrison, and F. Solzbacher, "Preliminary study of the thermal impact of a microelectrode array implanted in the brain," in *Proc. International Conference of the IEEE*, 2006.

[28] L. Tychsen, "Binocular vision," in *Adler's Physiology of the Eye*, W. M. Hart, ed., St. Louis: Mosby Year Book, 1992. pp. 773-853.

[29] D. Yanai, *et al.*, "Visual performance using a retinal prosthesis in three subjects with retinitis pigmentosa," *Am. J. Ophthalmol.*, vol. 143, pp. 820-827, 2007.

[30] A. B. Majji, *et al.*, "Long-Term histological and electrophysiological results of an inactive epiretinal electrode array implantation in dogs," *Invest. Ophthalmol. Vis. Sci.*, vol. 40, no. 9, 1999.

[31] P. Walter and W. Mokwa, "Epiretinal visual prostheses," *Ophthalmologe*, vol. 102, no. 10, 2005.

[32] J. Duay, E. Gillette, R. Liu, and S. B. Lee, "Highly flexible pseudocapacitor based on freestanding heterogeneous MnO2/conductive polymer nanowire arrays," *Phys. Chem. Chem. Phys.*, vol. 14, pp. 3329-3337, 2012.

[33] M. Mahadevappa, J. D. Weiland, D. Yanai, and I. Fine, "Perceptual thresholds and electrode impedance in three retinal prosthesis subjects," *IEEE Transactions on Neural Systems and Rehabilitation Engineering*, vol. 13, no. 2, June 2005.

[34] R. Jensen and O. R. Ziv, "Thresholds for activation of rabbit retinal ganglion cells with relatively large, extracellular microelectrodes," *IOVS*, vol. 46, no. 4, 2005.

Diego Lujan Villarreal was born in Monterrey, Nuevo León, México in 1983. He received the B.S. degree in Mechatronics from the Monterrey Institute of Technology and Higher Education (ITESM) in 2006 and the M.S. degree in Microelectronics and Microsystems from the Hamburg University of Technology in 2010.

He has worked with the Cellular Therapy Department in the School of Medicine at ITESM, Monterrey, México, and he is now pursuing his PhD in the Institute of Nano and Medical Electronics at the Hamburg University of Technology, Hamburg, Germany. His main research interests focus on theoretical models of neurostimulation, optimal energy-saving algorithms and epi- and sub retinal stimulation.

Dietmar Schroeder (M'88–SM'94) received the Dr. Ing. degree in electrical engineering from the Technische Universität Braunschweig, Braunschweig, Germany, in 1984. He joined the Hamburg University of Technology, Hamburg, Germany, in 1983, where he has been a Lecturer with Semiconductor Electronics since 1994.

Wolfgang H. Krautschneider (M'85) received the M.Sc., Ph.D., and Habilitation degrees from the Berlin University of Technology, Berlin, Germany. He was with Central Research Laboratories, IBM, Yorktown Heights, NY, USA, the Siemens Research Center, Munich, Germany, and the DRAM Project of IBM and Siemens, Essex Junction, VT, USA. He is currently the Head of the Institute of Nano and Medical Electronics at the Hamburg University of Technology, Hamburg, Germany.